17th World Conference on Earthquake Engineering, 17WCEE
Sendai, Japan - September 13th to 18th 2020

PARAMETER OPTIMIZATION FOR STIFFNESS DISTRIBUTION AND DAMPING COEFFICIENT DISTRIBUTION IN A GROUP OF BUILDINGS

T. Sone[(1)], T. Kinoshita[(2)], M. Yamamoto[(3)]

[(1)] *Chief Researcher, Research and Development Institute, Takenaka Corporation, sone.takayuki@takenaka.co.jp*
[(2)] *Associate Chief Researcher, Research and Development Institute, Takenaka Corporation, kinoshita.takuya@takenaka.co.jp*
[(3)] *General Manager, Earthquake Engineering Department, Research and Development Institute, Takenaka Corporation, yamamoto.masashia@takenaka.co.jp*

Abstract

The advances in computational design have been remarkable, and it has begun to be widely used even in the building design field in Japan. The driving force for the spread of this design method is the availability of versatile related software. By using such software, optimization techniques such as genetic algorithm can be easily utilized. Also, global and Pareto optimal solutions depending on the objective functions defined by users can be efficiently explored. Engineering support through optimization techniques helps designers quickly find better solutions to a variety of problems. Moreover, the discovery of innovative and rational elements missing in conventional designs can be expected. The authors are hopeful in the potentiality of the computational design, and attempted to explore structural control systems by utilizing optimization techniques. This paper presents the results of a study focusing on a group consisting of two high-rise and two low-rise buildings. Referring to some actual adjacent buildings that were integrated together by connecting each other, the study model was established so that it could add four additional layers at the bottom of each building and four additional connecting members between adjacent buildings. The model was subjected to various input ground motions, including artificial seismic waves of large-amplitude ground motions caused by the Nankai megathrust earthquake and the Uemachi fault belt, which raise serious concern in Japan. The optimization calculation was performed considering the stiffness and damping coefficients of the study model as design variables. Based on the responses of floor accelerations, inter-story drifts of superstructures, and relative deformations of additional layers, the qualitative characteristics of the solutions are discussed. The results suggest that the structural system connecting the respective first floors of the four buildings with a rigid member and having the low stiffness and high damping coefficients in the additional bottom layers is qualitatively superior; the system is regarded as an integrated seismically isolated structure with “ultra-long natural period” and “ultra-high damping” characteristics, which are advantageous.

Keywords: discrete optimization; genetic algorithm; large-amplitude ground motion; ultra-long natural period; ultra-high damping

1. Introduction

The advances in computational design have been remarkable, and it has begun to be widely used even in the building design field in Japan [1, 2]. The driving force for the spread of this design method is the availability of versatile related software. By using this software, optimization techniques such as genetic algorithm (GA) can be easily utilized. Also, global and Pareto optimal solutions depending on the objective functions defined by users can be efficiently explored. Engineering support through the optimization techniques helps designers quickly find better solutions to a variety of problems. Moreover, the discovery of innovative and rational elements missing in conventional designs can be expected.

The 2011 Great East Japan Earthquake is still fresh in our memory; the earthquake caused not only devastating damage to the vast areas of East Japan but also long-duration vibrations in high-rise buildings in Tokyo and Osaka, which were far from the epicenter [3]. Currently, the occurrence of a massive earthquake with hypocenter along the Nankai trough (hereinafter called "Nankai megathrust earthquake") is a serious concern in Japan. The earthquake magnitude of the Nankai megathrust earthquake is believed to be comparable to that of the 2011 Great East Japan Earthquake, and it is suggested that the long-period component of seismic ground motions may significantly exceed that of the artificial design wave for the structural design in Japan. On the other hand, there is also concern regarding potential inland earthquakes in urban areas such as Tokyo and Osaka. In particular, it is suggested that a near-fault earthquake caused by the Uemachi fault belt in Osaka may result in fatal damage to many buildings. Taking countermeasures against these tremendous ground motions (hereinafter called "large-amplitude ground motions") is an urgent issue in Japan. Various countermeasures such as increasing the capacity of oil dampers to achieve highly damped structures [4] and installing huge mass dampers for seismic retrofitting of an existing high-rise building [5] have been taken.

While considering countermeasures against large-amplitude ground motions, the authors are hopeful in the potentiality of the computational design, and attempt to explore structural control systems by utilizing optimization techniques. This paper presents the results of a study on a group consisting of two high-rise and two low-rise buildings. For multiple seismic ground motions, including artificial seismic waves of large-amplitude ground motions caused by the Nankai megathrust earthquake and the Uemachi fault belt, the qualitative characteristics of superior solutions discovered by using the optimization techniques are demonstrated.

2. Setting up optimization problems

2.1 Study model and design variables

In recent years, several groups of buildings have been designed integrally by connecting the same floor of multiple adjacent buildings [6-9]. As an approach to exploring the high seismic performance of structural systems for such a group of buildings, we considered a group of adjacent buildings, including the two 18-story buildings and two 6-story buildings shown in Fig. 1a, and performed a discrete optimization for the stiffness and the damping coefficients of the study model shown in Fig. 1b. In the discrete optimization, increasing the number of design variables and the number of values that can be taken in each design variable leads to an exponential increase of the computational load. Therefore, as shown in Fig. 1a, we modeled each of the four buildings as a lumped mass model in which three floors, each with a height of 4.5 m, were condensed into one lumped mass. In addition, referring to some actual adjacent buildings that were integrated together by connecting each other, the study model shown in Fig. 1b was established so that it could add four additional layers at the bottom of each building and four additional connecting members between adjacent buildings.

The design variables in the optimization, stiffness *Kf*, *Ki*, and *Kc*, and damping coefficients *Ci* and *Cc*, are shown in Fig. 1b. The damping coefficient *Cf* is defined as a function of the stiffness *Kf*, as later described. We demonstrate in advance that the total number of combinations considering all design variables is 3.32×10^{29}, which is a very large number.

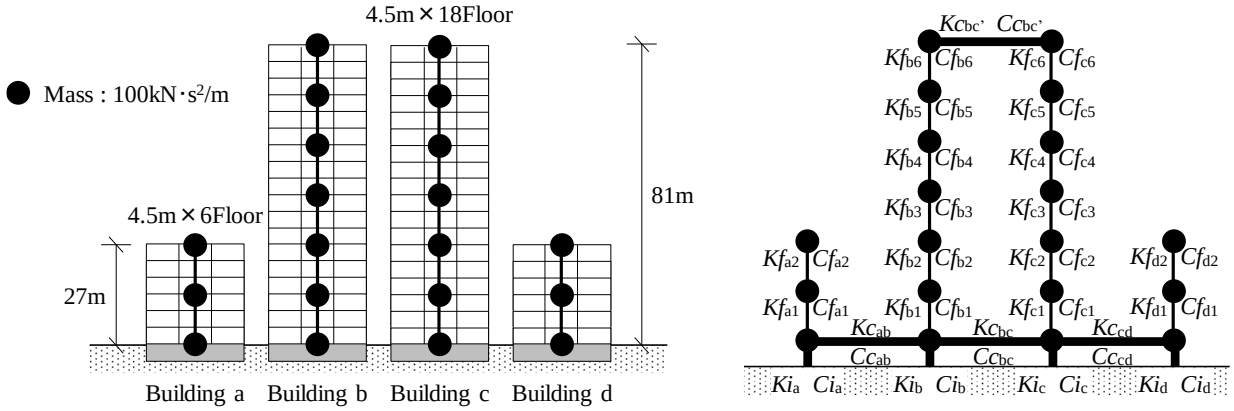

(a) Assumed adjacent buildings (b) Target model for the optimization

Fig. 1 – Study model

The values of the stiffness *Kf* and the damping coefficient *Cf* in each building were set as follows. First, the reference stiffness Kf_0 were defined, of which the value was 17,000 kN/m. In addition, the reference damping coefficient Cf_0 was also defined, of which the value was 84.4 kN·s/m for buildings "a" and "d", and 216 kN·s/m for buildings "b" and "c". When these values are set for each lumped mass model in Fig. 1a, the values of the first natural period in the case that each first floor was fixed are 0.78 seconds for buildings "a" and "d", and 2.0 seconds for buildings "b" and "c", and each value of the first modal damping ratio is 2.0%. Based on the reference values, seven different values of the stiffness *Kf* were selected within a range of 1/3 to 3 times the reference value Kf_0 (Table 1a). The value of the damping coefficient *Cf* was calculated from the equation $Cf_0 \cdot \sqrt{Kf/Kf_0}$ for each story element. If a value of *Kf* is selected arbitrary, and the stiffness and corresponding damping coefficient are given at all story elements of each lumped mass model shown in Fig. 1a, the value of the first modal damping ration in the case that the first floor was fixed is 2.0%.

The values of the stiffness *Ki* and the damping coefficient *Ci* in the additional layers were set as follows (Table 1b). These layers were considered from a range of structural specifications, which could be selected widely from a small to large value. Ten different values were selected of stiffness *Ki* within a range that the natural period of a single degree of freedom (SDOF) model was to be 0.1 to 20 seconds. Here, the mass of the SDOF model is 700 kN·s^2/m, and the value corresponds to the total weight of the building "b". Additionally, considering the stiffness of the SDOF model as 276 kN/m, which means that the natural period of the SDOF model is 10 seconds, ten different values of the damping coefficient *Ci* were selected within the range of the damping coefficients that the damping ratio of the SDOF model was 0 to 80%.

The values of the stiffness *Kc* and the damping coefficient *Cc* in the connecting members were set as follows (Table 1c). These members were considered from a range of structural specifications, which could be selected widely from a small to large value. Ten different values were selected of the stiffness *Kc* within a range that the natural period of the SDOF model with a mass of 700 kN·s^2/m was to be 0.1 to 100 seconds. When the value of 2.76 kN/m, which is the minimum value of *Kc*, was selected, the state of no connection between adjacent buildings could be roughly simulated. The values of the damping coefficient *Cc* were the same as those of the damping coefficient *Ci*.

Table 1 – Design variables

(a) Stiffness *Kf*

	1	2	3	4	5	6	7
*Kf** (×10^{3}kN/m)	5.67 (0.33)	11.3 (0.67)	17.0 (1.00)	25.5 (1.50)	34.0 (2.00)	42.5 (2.50)	51.0 (3.00)

(b) Stiffness *Ki* and damping coefficient *Ci*

	1	2	3	4	5	6	7	8	9	10
Ki† (×10^{3}kN/m)	6.91×10^{-2} (20)	0.276 (10)	0.564 (7.0)	1.11 (5.0)	1.73 (4.0)	3.07 (3.0)	6.91 (2.0)	27.6 (1.0)	111 (0.5)	2.76×10^3 (0.1)
Ci‡ (kN･s/m)	0.00 (0.0)	17.6 (2.0)	35.2 (4.0)	52.8 (6.0)	70.4 (8.0)	88.0 (10)	176 (20)	352 (40)	528 (60)	704 (80)

(c) Stiffness *Kc* and damping coefficient *Cc*

	1	2	3	4	5	6	7	8	9	10
Kc† (×10^{3}kN/m)	2.76×10^{-3} (100)	0.276 (10)	1.11 (5.0)	3.07 (3.0)	6.91 (2.0)	27.6 (1.0)	56.4 (0.7)	111 (0.5)	307 (0.3)	2.76×10^3 (0.1)
Cc‡ (kN･s/m)	0.00 (0.0)	17.6 (2.0)	35.2 (4.0)	52.8 (6.0)	70.4 (8.0)	88.0 (10)	176 (20)	352 (40)	528 (60)	704 (80)

*: The number in parentheses shows the value of Kf/Kf_0.

†: The number in parentheses shows the period (s) for the SDOF model with a mass of 700 kN･s^2/m.

‡: The number in parentheses shows the damping ratio (%) for the SDOF model with a mass of 700 kN･s^2/m and the stiffness of 276 kN/m.

2.2 Input ground motions

Assuming that the site is the Osaka Bay Area in Japan, a total of 14 artificial seismic waves shown in Table 2 were selected as input ground motions for the study. The waves include design waves assuming large-amplitude ground motions caused by massive earthquakes, which have raised concerns at the site. The OS wave is an artificial seismic wave on the engineering bedrock predicting occurrences generated by the Nankai megathrust earthquake. The wave data was calculated and released to the public by the Japanese Ministry of Land, Infrastructure, Transport, and Tourism [10]. The amplification of motions in the long-period component owing to the surface strata characteristic is assumed to be small, and the amplification of the OS wave by the surface strata is not considered in this study. At the time of the 2011 Great East Japan Earthquake, ground accelerations were observed at Konohana located in the Osaka Bay Area through the KiK-net, which is one of the strong-motion seismograph networks by the National Research Institute for Earth Science and Disaster Resilience (NIED) in Japan. Assuming ground motions caused by the Nankai megathrust earthquake as with the OS wave, the KK waves were calculated by multiplying the observation data at Konohana by a factor α. Theoretically, the amplitude of both the body wave and surface wave is attenuated by the ratio $1/r$ and $1/\sqrt{r}$, for the distance r from the hypocenter to the site, respectively. Here, considering the effect of the attenuation relationship for the body wave to be a safe evaluation, the ratio r_1/r_2 of the distance r_1 from the Konohana observation point to the hypocenter of the 2011 Great East Japan Earthquake to the distance r_2 from the Konohana observation point to the hypocenter of the Nankai megathrust earthquake was applied as the above amplification factor α: where the value is 4.59. The UF and UP waves are artificial seismic waves predicting occurrences generated by a near-fault earthquake caused by the Uemachi fault belt in Osaka. These wave data were calculated and released to the public by the Kansai branch of the Japan Structural Consultants Association (JSCA) [11]. A unique feature of the UF waves is that the curve of their relative velocity response spectrum is almost flat in the long-period region. A distinctive feature of the UP waves is that the magnitude of their

dominant period component is strong and their wave form is like pulse. The JA waves are the artificial seismic waves for the assumed site, which correspond to the extremely rare level (level 2) wave stipulated in the notification of the Building Standard Law of Japan. They were calculated by adopting the phase in the observation wave of the 2004 off the Kii Peninsula earthquake, of which the long-period component was dominant.

Table 2 – PGA and PGV of input ground motions

	Time Duration (s)	PGA (m/s^2)	PGV (m/s)
OS	655.36	0.263	0.467
KK1	279	0.068	0.478
KK2	279	0.074	0.519
UF1	40.96	0.711	1.346
UF2	40.96	0.694	1.766
UF3	40.96	0.588	1.476

	Time Duration (s)	PGA (m/s^2)	PGV (m/s)
UP1	40.96	0.226	1.107
UP2	40.96	0.391	1.265
UP3	40.96	0.362	1.047
UP4	40.96	0.253	0.776
UP5	40.96	0.199	0.806
UP6	40.96	0.230	0.758
JA1	200	0.316	0.638
JA2	200	0.273	0.615

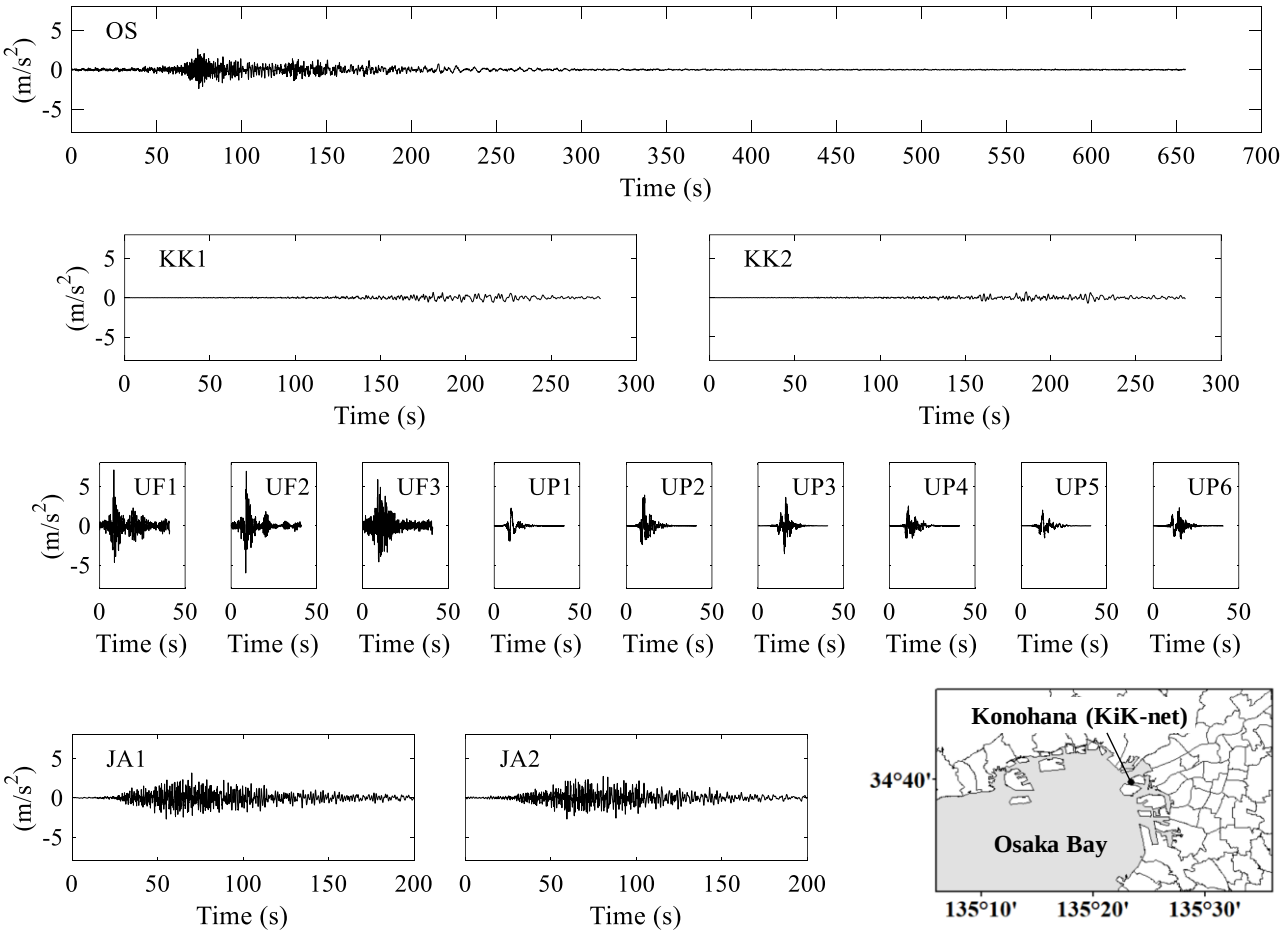

Fig. 2 – Acceleration waveforms of input ground motions

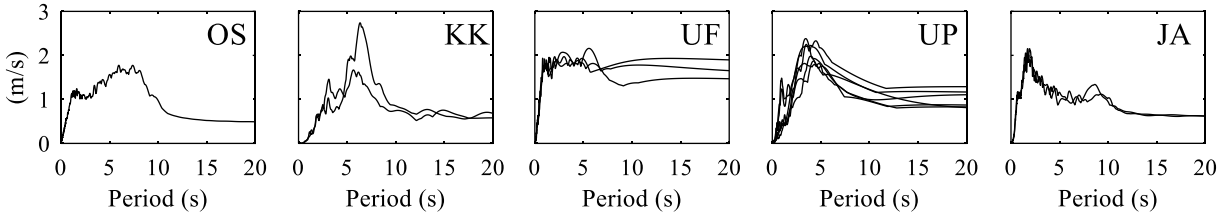

Fig. 3 – Relative velocity response spectra for 5% damping of input ground motions

The acceleration waveform of each input ground motion and the corresponding relative velocity response spectrum for 5% damping are shown in Figs. 2 and 3, respectively. As reference results of the response for the 14 waves, the maximum floor acceleration A_{max} and the maximum inter-story drift δ_{max} of each Base Fixed Structure model (BFS model) are shown in Table 3. The BFS models are four lumped mass models shown in Fig. 1a where each first floor is fixed. They are given a stiffness Kf_0 at all story elements. Additionally, a stiffness proportional damping with the first modal damping ratio of 5% is set for each BFS model. Furthermore, A_{max}, δ_{max} and maximum deformation D_{max} of the additional basement layer of each Seismically Isolated Structure model (SIS model) are also shown in Table 3. The SIS models are four lumped mass models shown in Fig. 1a with an additional basement layer below each building. They are given a stiffness Kf_0 and a damping coefficient Cf_0 at all story elements, but the stiffness and damping coefficient of each additional basement layer are set to be at the natural period- 4.0 seconds, and damping ratio- 20%, when considering each superstructure as a rigid body.

Table 3 – Maximum responses of BFS models and SIS models

	BFS model		SIS model	
	Building a and d	Building b and c	Building a and d	Building b and c
A_{max} (m/s^2)	16.0	8.99	2.77	3.81
δ_{max} (mm)	150	176	30	85
D_{max} (m)	-	-	0.90	0.87

2.3 Optimization calculation

The discrete optimization calculation was performed using the commercial software "modeFRONTIER®". The MOGA-II, which is one of the multi-objective genetic algorithm (MOGA) that is effective for discrete optimization [12], was applied. The number of individuals in the initial population was 100, and the optimization calculation was performed for up to 100 generations. In the configuration of the MOGA-II algorithm, the generational evolution was selected. The probability of the directional cross-over was 0.5, the probability of the selection was 0.05, the probability of the mutation was 0.1, and the DNA string mutation ratio was 0.05. Also, the elitism was enabled.

In the optimization, the minimization of three kinds of maximum responses resulting from the above-mentioned input of ground motions was conducted; those responses are the maximum floor acceleration A_{max} in all floors, the maximum inter-story drift δ_{max} in all building stories, and the maximum deformation D_{max} in all additional layers. Here, the objective functions f_1, f_2, and f_3 shown in Fig. 4 were defined, considering the value of each maximum response as a variable. Each objective function has a bending point, and its value in the horizontal axis is 2.0 m/s^2 (A_{cr}) in the function f_1, 67.5 mm (δ_{cr}) in the function f_2, and 0.6 m (D_{cr}) in the function f_3; the value of δ_{cr} corresponds to the inter-story drift angle of 1/200 because the height between mass nodes is 13.5 m. The A_{cr}, δ_{cr}, and D_{cr} values were determined by considering the conventional response criterion of a seismically isolated building for the level 2 design waves in Japan. In this study, we adopted these A_{cr}, δ_{cr}, and D_{cr} values as the target responses for exploring the structural system against the input ground

motions, including large-amplitude ground motions. By adopting these objective functions, the solutions with smaller maximum responses than the A_{cr}, δ_{cr}, and D_{cr} values are considered to be easier to find.

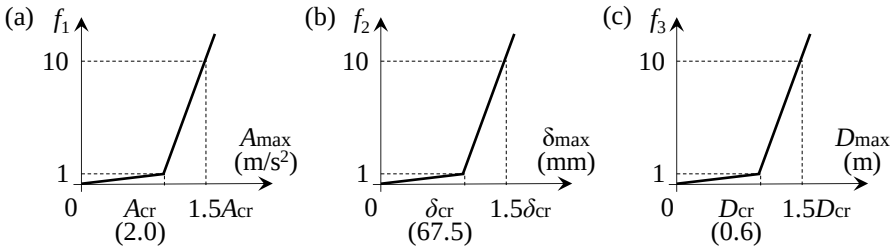

Fig. 4 – Objective functions

3. Results of optimization calculation

3.1 Distribution of solutions on response surface

First, we investigate the distribution of the solutions on the response surface. On the solutions selected by the optimization calculation, the relationships between the D_{max} and A_{max}, the D_{max} and δ_{max}, and the A_{max} and δ_{max} are shown in Fig. 5. The plots in each figure are classified into three groups (Group 1: T_1 < 5.0 seconds, Group 2: 5.0 seconds ≤ T_1 < 10.0 seconds, Group 3: 10.0 seconds ≤ T_1) according to the value of the first natural period T_1 for each solution obtained from the real eigenvalue analysis. The two dotted lines in each figure represent the positions of the A_{cr}, δ_{cr}, and D_{cr} values defined in Fig. 4, respectively. As for references, the response results of the BFS models and the SIS models shown in Table 3 are plotted with white circles in each figure, but the response results of the BFS models are mostly out of display range.

Focusing on Figs. 5a and 5b, Pareto optimal solutions that show a trade-off relationship are found in the region- D_{max} ≤ approximately 1.0 m. On the other hand, the plots in Fig. 5c disperse radially from the origin, and the plots around the origin are considered as a solution where the D_{max} value is approximately 1.0 m. Comparing the difference between the distributions of the three types of groups mentioned above, as the value of T_1 for a solution becomes longer, the minimum values of the A_{max} and δ_{max} values tend to be smaller. The results of Group 1 in Fig. 5c could not obtain the solutions that satisfy $A_{max} \leq A_{cr}$ and $\delta_{max} \leq \delta_{cr}$. It is necessary to ensure 5.0 seconds ≤ T_1 in order to realize the solutions that satisfy $A_{max} \leq A_{cr}$ and $\delta_{max} \leq \delta_{cr}$ for the input ground motions.

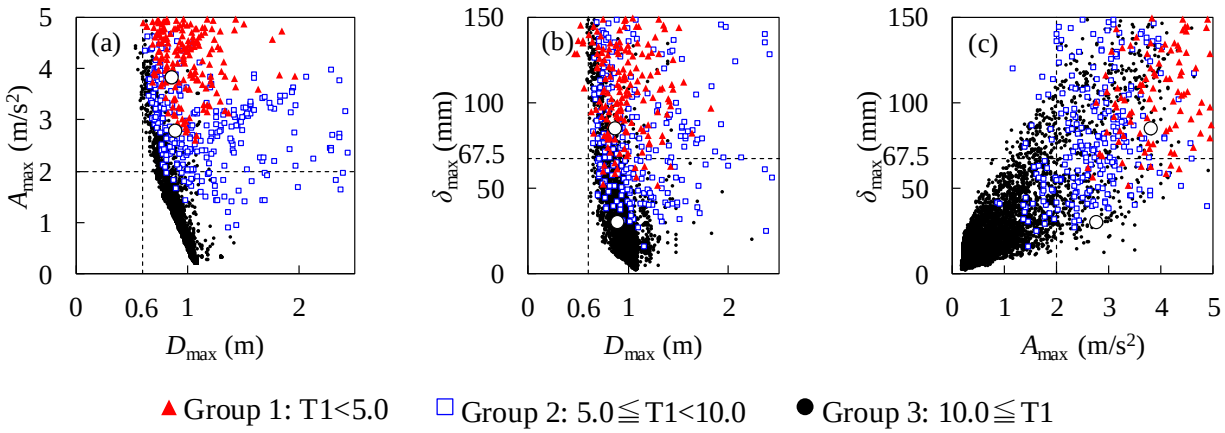

Fig. 5 – Distributions of solutions on response surfaces

3.2 Characteristics of solutions with minimum values of A_{max} and δ_{max}

Based on the results in Fig. 5a and 5b, by allowing the deformation exceeding the D_{cr} value to additional layers, the A_{max} and δ_{max} values can be minimized in the optimization calculation. Under the assumption that the structural system can accept the D_{max} exceeding the D_{cr} value, a set of 100 solutions corresponding to the plots near the origin in Fig. 5c (hereinafter called "Group A") were extracted, and the characteristics of the solutions were examined. The frequency distribution of selected values in each design variable in Group A is shown in Fig. 6. The maximum display length of bars corresponds to the 100 solutions, and the bars showing the maximum frequency in each design variable are depicted in black. Fig. 6 shows that only the minimum value for the stiffness *Ki* (69.1 kN/m in Table 1b) is selected. Moreover, the minimum value for the damping coefficient *Ci* (0 kN·s/m in Table 1b) and the value close to the maximum value for the stiffness *Kc* (2.76×10^6 kN/m in Table 1c) tend to be selected.

Referring to the results in Fig. 6, we determined a model setting the values shown in Fig. 7a for each design variable (hereinafter called "Model A"). The first natural period of Model A obtained from the real eigenvalue analysis is approximately 17 seconds, which seems to be a very long natural period. Two types of transfer functions on Model A are shown in Fig. 7b. One is the transfer function of the absolute acceleration (TFA) at the first floor and the top of the building "b" with respect to the ground motion acceleration. The other is the transfer function of the relative displacement (TFD) at the first floor and the top of the building "b" with respect to the ground motion displacement. In the TFA shown in Fig. 7b, a sharp peak appears at the long period of 17 seconds, but the magnification in the period range of 10 seconds or less is much smaller than 1.0; therefore, most of the main vibration components on the ground acceleration are not transferred to the building. The magnification of the TFD in a period range of 10 seconds or less is almost 1.0, and the curve at the first floor is identical with that at the top; therefore, the maximum deformation of the additional layer approaches the value of the ground motion itself, and almost no inter-story drift in the building appears. Comprehensively, the structural system that completely isolates buildings from the ground may have been qualitatively estimated to be superior in the optimization calculation. Though this paper doesn't demonstrate this, it has been separately confirmed that changing the stiffness distributions of both "b" and "c" buildings does not significantly contribute to the responses, since the main vibration components on the ground motion acceleration to the building were almost eliminated owing to the characteristics of Model A. Incidentally, for the input ground motions, the A_{max} value of Model A was 0.193 m/s^2, the δ_{max} value was 2.24 mm and the D_{max} value was 1.10 m.

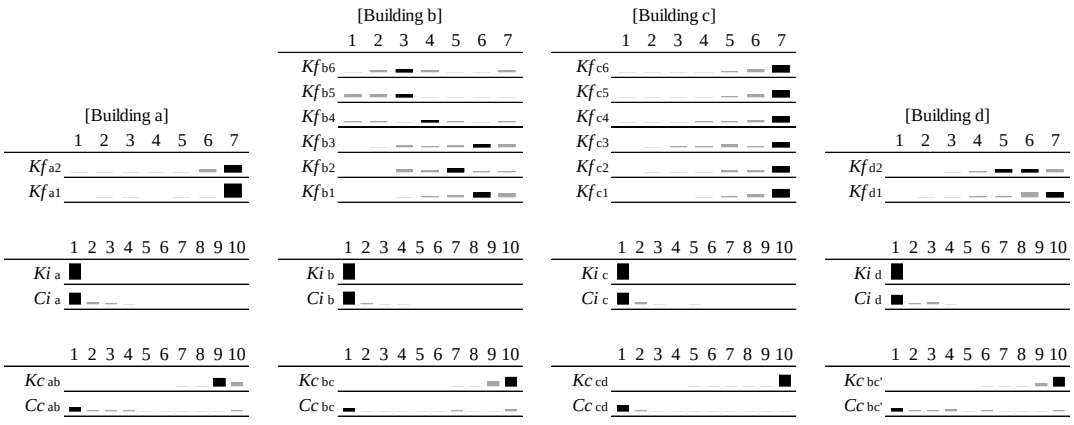

Fig. 6 – Frequency distribution of selected values in each design variable in Group A

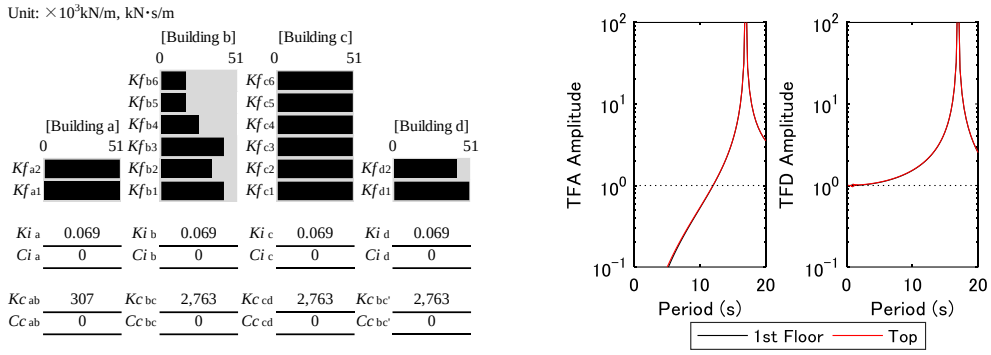

(a) Structural specifications (b) TFA and TFD of the building "b"

Fig. 7 – Structural specifications of Model A and corresponding transfer functions

3.3 Characteristics of solutions with A_{max} and δ_{max} values less than A_{cr} and δ_{cr} values

It is not reasonable to make layers or members to withstand a large deformation exceeding 1.0 m. Therefore, secondarily, a solution that satisfies small responses less than two target responses A_{cr} and δ_{cr} while keeping the D_{max} value as small as possible was sought. Fig. 8 shows the relationship between the A_{max} and δ_{max} values, but the plots are classified into five groups according to the D_{max} value. The two dotted lines in each figure represent the positions of the A_{cr} and δ_{cr} values, respectively. The solutions with the results- D_{max} < 0.7 m shown in Fig. 8a does not satisfy $A_{max} \leq A_{cr}$ and $\delta_{max} \leq \delta_{cr}$. The results suggest the necessity to provide additional layers to deform more than 0.7 m exceeding the value of the D_{cr} for the input ground motions.

In Fig. 8b, 47 plots that satisfied the relationships of $A_{max} \leq A_{cr}$ and $\delta_{max} \leq \delta_{cr}$ (hereinafter called "Group B") were extracted, and were depicted with white circles. The frequency distribution of selected values in each design variable in Group B is shown in Fig. 9. The maximum display length of bars corresponds to the 47 solutions, and the bars showing the maximum frequency in each design variable are depicted in black. Similar to the results in Fig. 6, only the minimum value in Table 1b is selected for the stiffness *Ki*. On the other hand, various values are selected for the damping coefficient *Ci*, but relatively large values tend to be selected except for the damping coefficient Ci_c. The value of the stiffness *Kc* is selected to be close to the maximum value in Table 1c, and thus, the value of the damping coefficient *Cc* has little effect on the responses.

Since the very large values for the stiffness Kc_{ab}, Kc_{bc}, and Kc_{cd} tend to be selected, the connecting members on much of the solutions behave almost as rigid bodies, and the additional layers of four buildings move together. It means that the feature is characterized by the sum of values of the stiffness *Ki* and the sum of values of the damping coefficient *Ci*. Fig. 10 shows the frequency distributions of the total stiffness Σ*Ki*, the total damping coefficient Σ*Ci*, and the ratio Σ*Ci*/Σ*Ki* in Group B, respectively. The Σ*Ci*/Σ*Ki* values are generally distributed between 4.0 seconds and 6.0 seconds.

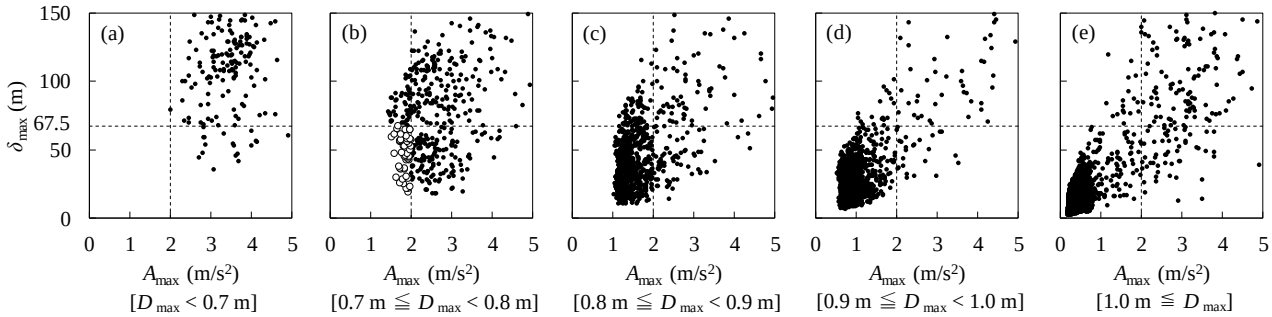

Fig. 8 – Relationship between A_{max} and δ_{max}

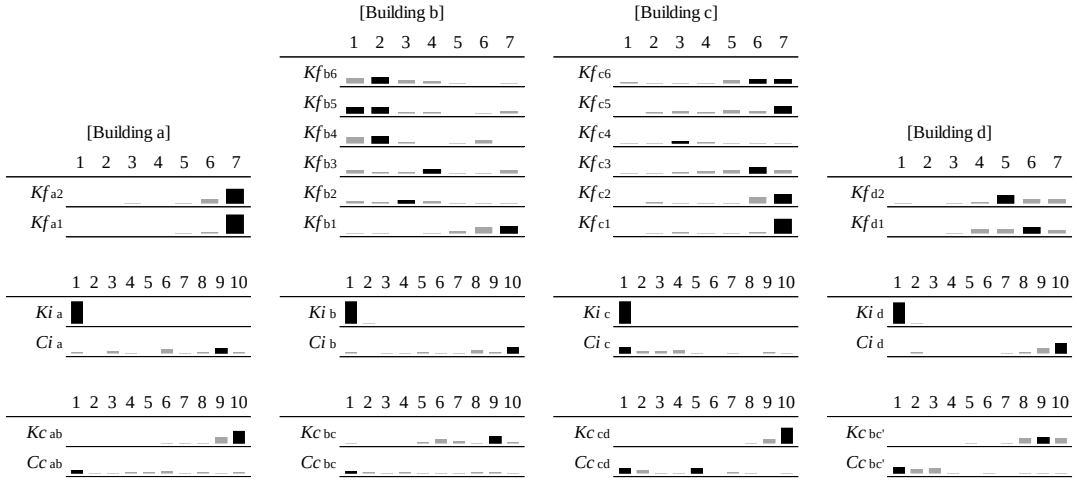

Fig. 9 – Frequency distribution of selected values in each design variable in Group B

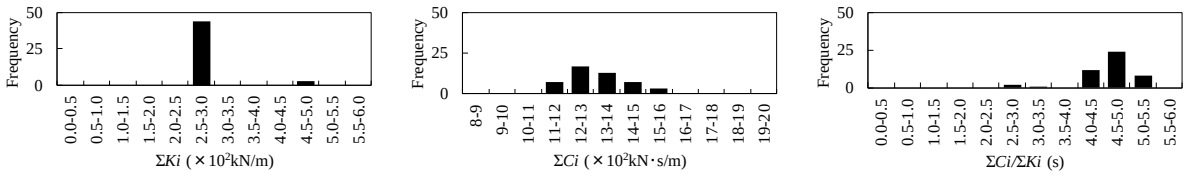

Fig. 10 – Frequency distributions of Σ*Ki*, Σ*Ci*, and Σ*Ci*/Σ*Ki* values in Group B

Considering the results of Figs. 9 and 10, a model setting the values shown in Fig. 11a was drawn up for each design variable (called "Model B" from now on). Here, the value of the damping coefficient *Ci* was selected so that the value of the ratio Σ*Ci*/Σ*Ki* was 4.5 seconds. Because the value of the stiffness Kc_{ab}, Kc_{bc}, and Kc_{cd} are extremely large, and the additional layers of four buildings move together, the arrangement of the four values of the damping coefficient *Ci* was arbitrarily determined. It is difficult to distinguish the predominant values of the stiffness *Kf* in the buildings "b" and "c" from the result in Fig. 9. Therefore, a set of values of the stiffness $\{Kf_{b1}, \cdots, Kf_{b6}, Kf_{c1}, \cdots, Kf_{c6}, Kc_{bc'}\}$ were separately searched for with the highest correlation with 47 solutions in Group B, and the results are shown in Fig. 11a. The first natural period obtained from the complex eigenvalue analysis of Model B is 16.8 seconds, and the first modal damping ratio is 82.8%; the result indicates the superiority of the ultra-long natural period and ultra-high damping characteristics that are not familiar in the conventional structural design. In the optimization, without taking into account the cost, it was not clear why the stiffness *Kf* of the superstructure tends to be selected as the small value at the upper stories in the building "b" and the large value in the building "c" as shown in Figures 6 and 9. Similarly, it was also not clear why the tops of the buildings "b" and "c" tend to be connected by a rigid member. The transfer functions TFA and TFD on Model B are shown in Fig. 11b. In contrast to the characteristics shown in Fig. 7b, no peak is seen in the period range of 10 seconds or more. Since the second natural period of Model B is 1.1 seconds and its modal damping ratio is approximately 7%, the peaks appearing in the period range around 1.1 seconds on both transfer functions are considered as the response by the second mode.

The maximum floor accelerations and the inter-story drifts of the four buildings in Model B for the input ground motions are shown in Fig. 12. As for references, we also show the responses of both Model X and Model Y. In Model X, the stiffness $Kc_{bc'}$ value in Model B is replaced with the minimum value in Table 1c, and in Model Y, the stiffness *Kf* values of the four buildings in Model B are replaced with the maximum value

in Table 1a. Comparing the results of Model B and Model X, it founds that the rigid member connecting the tops of the buildings "b" and "c" is effective on the inter-story drift of the building "b." The superiority of Model B over Model Y is not obvious. Incidentally, the response of the D_{max} is 0.786 m for Model B, 0.783 m for Model X, and 0.792 m for Model Y, and the relative displacement between the tops of the buildings "b" and "c" in Model X is 144 mm.

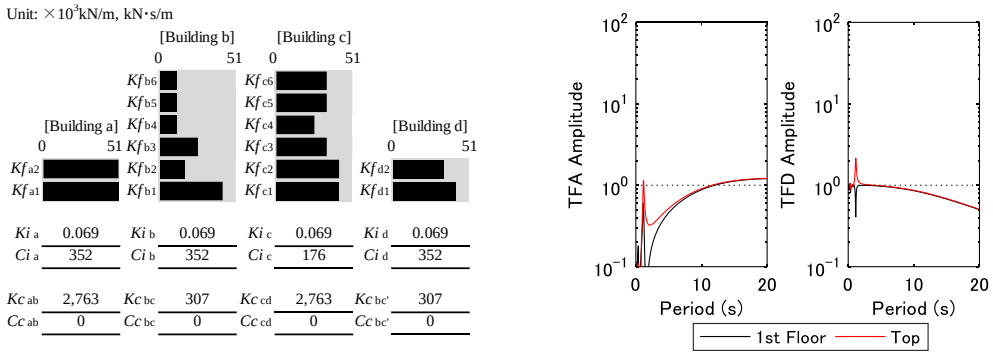

(a) Structural specifications (b) TFA and TFD of the building "b"

Fig. 11 – Structural specifications of Model B and corresponding transfer functions

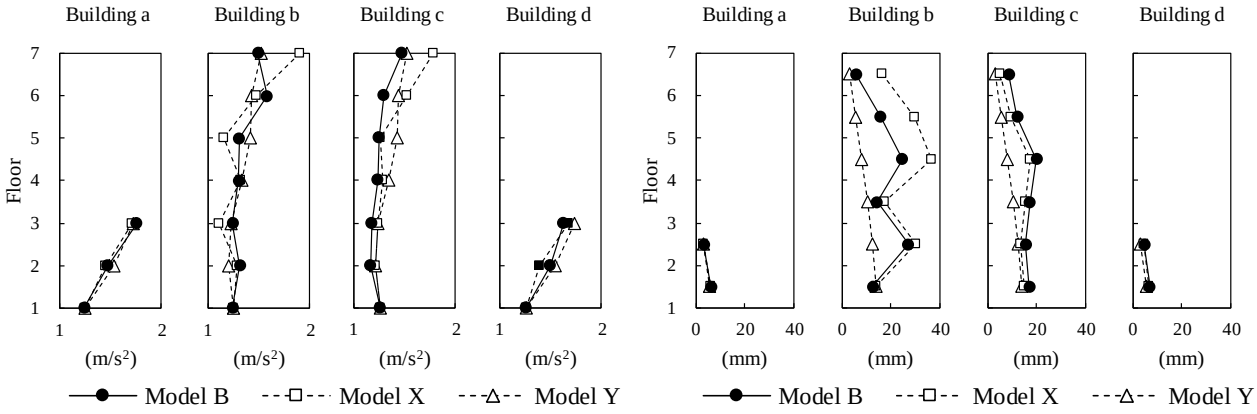

(a) Maximum floor acceleration (b) Inter-story drift

Fig. 12 – Comparison with the maximum responses among Model B, Model X, and Model Y

4. Concluding remarks

By utilizing optimization techniques, the authors have attempted to explore structural control systems against large-amplitude ground motions. In this paper, two high-rise buildings and two low-rise buildings adjacent to each other were considered, and the discrete optimization was performed considering the stiffness and the damping coefficient of the buildings as design variables. The results of the study are summarized below.

- In order to realize the solutions that satisfy $A_{max} \leq A_{cr}$ and $\delta_{max} \leq \delta_{cr}$ for the input ground motions, it is necessary to ensure that 5.0 seconds $\leq T_1$ and the additional layer deforms more than 0.7 m.
- If the additional layer can be allowed to be deformed by more than 1.0 m, the structural system can minimize the A_{max} and δ_{max} values for the input ground motions. The system has the advantages of "ultra-long natural period" and "extremely low damping", and is considered to be equivalent to the system that isolates the building from the ground completely. Although not described in this paper, it should be noted that the long-period and large sway motion may continue after the earthquake since the damping ratio is almost 0.0%.

- In order to satisfy $A_{max} \leq A_{cr}$ and $\delta_{max} \leq \delta_{cr}$ while keeping the D_{max} value within 0.8 m for the study model, the structural system connecting the respective first floors of the four buildings with a rigid member and having the low stiffness and high damping coefficients in the additional bottom layers is qualitatively superior. The system is regarded as an integrated seismically isolated structure with "ultra-long natural period" and "ultra-high damping" characteristics, which are advantageous.

These results suggest the necessity of a structural system with a novel concept in order to resist large-amplitude ground motions. From a practical point of view, there are various issues to address in the existing structural system. In addition, further research on the vibration component of the ground motion in the range of periods exceeding 10 seconds will be necessary. However, the authors conclude that the structural system demonstrated in this study could serve as a countermeasure to overcome the threat of large-amplitude ground motions in Japan.

5. Acknowledgements

We utilized the observation data of the KiK-net by the National Research Institute for Earth Science and Disaster Prevention, NIED. We would like to thank Mr. Haruo Yoshida of the Research & Development Institute, Takenaka Corporation, for his technical support on the input ground motions.

6. References

[1] Januszkiewiczl K, Banachowicz M (2017): Nonlinear shaping architecture designed with using evolutionary structural optimization tools. *IOP Conference Series: Materials Science and Engineering*, **245**, 082042.

[2] ESTECO (2019). Success story: Takenaka Corporation automates simulation-based architectural design, available at https://www.esteco.com/cmis/browser?id=workspace://SpacesStore/b8e423c7-bd8c-4962-b342-13c820cc719a (last accessed 17 January 2020).

[3] Çelebi M, Kashima T, Ghahari SF, Koyama S, Taciroğlu E, Okawa I (2017): Before and after retrofit behavior and performance of a 55-story tall building inferred from distant earthquake and ambient vibration data. *Earthquake Spectra*, **33**(4), 1599-1626.

[4] Yamamoto M, Minewaki S, Nakahara M, Tsuyuki Y (2016): Concept and performance testing of a high-capacity oil damper comprising multiple damper units. *Earthquake Engineering & Structural Dynamics*, **45**(12), 1919-1933.

[5] Sone T, Ogino K, Kamoshita N, Muto K, Ide Y, Murata K, Hamaguchi H, Yamamoto M (2019): Experimental verification of a tuned mass damper system with two-phase support mechanism. *Japan Architectural Review*, **2**(3), 250-258.

[6] Wood A, Safarik D (2019): Skybridges: A history and a view to the near future. *International Journal of High-Rise Buildings*, **8** (1), 1-18.

[7] Nishimura A (2011): Vibration control of a tower complex connected by sky gardens. *CTBUH Journal*, II, 30-35.

[8] Lioe R, Wong W, McNiven B, Wu X, Mak B (2012): The Sands hotel and Sands sky park. *The Arup Journal*, 1, 17-30, Arup.

[9] Lago A, Trabucco D, Wood A (2018): *Damping Technologies for Tall Buildings: Theory, Design, Guidance and Case Studies*. Elsevier, 818-827.

[10] Japanese Ministry of Land, Infrastructure, Transport, and Tourism (MLIT) (2015). Public comment on "Measures for long-period ground motions due to extreme earthquakes along the Nankai Trough in high-rise buildings" (in Japanese), available at http://www.mlit.go.jp/report/press/house05_hh_000601.html (last accessed 17 January 2020).

[11] Research Group about Design Earthquake Ground Motion and Design Method of Building for Inland Earthquake underneath the Osaka Area (2015): *Design Earthquake Ground Motion and Aseismic Design Guideline of Building for Inland Earthquake underneath the Osaka Area*. JSCA Kansai (in Japanese).

[12] Poles S (2003): MOGA- II – An improved multi-objective genetic algorithm. *ESTECO Technical Report 2003-006*, ESTECO.

